J Mater Sci (2021) 56:5670–5683

Computation & theory

The rigidizable behavior of the deployable hindwings of the Asian ladybeetle during flight

Zelai Song[1], Jin Tong[1], Yongwei Yan[1], Limei Tian[1,*], and Jiyu Sun[1,*]

[1] *Key Laboratory of Bionic Engineering (Ministry of Education, China), Jilin University, Changchun 130022, People's Republic of China*

Received: 24 July 2020
Accepted: 22 November 2020
Published online: 3 January 2021

ABSTRACT

Deployable hindwings support the excellent flight performance of Coleoptera during flapping flight, exhibiting rigidizable behavior without refolding during flight. This paper investigates the inner structure of the veins of the Asian ladybird beetle (*Harmonia axyridis*) hindwing by histological sections and inverted fluorescence microscopy. Considering the hollow and solid structures of the veins and the wing membrane, two three-dimensional (3-D) models of the right hindwings are established for comparison: Model I with a solid C + ScA vein and Model II with a hollow C + ScA vein, and the other veins are solid. The relationships among the attack angles (− 60°, − 30°, 0°, 30° and 60°), locations at which the pressure is set and bending deformation tendencies of the two models are discussed. These related data are obtained by simulation. The results demonstrate that the hollow structures of the veins have a higher flexibility and self-adaption deformation than those of the solid veins, and sinusoidal relationships are observed between the resulting deformations and attack angles. The relationship between the rigidizable behavior of deployable hindwings and vein structure is discussed.

Introduction

Inspired by insect flight, people have recently designed flapping wing micro-aircraft that may be utilized for the folding/unfolding mechanism of larger flapping wing aircraft [1, 2]. The light mass and smart body design of a micro-air vehicle (MAV) are necessities, so many studies have been focused on researching and developing flapping wing micro-air vehicles (FWMAVs) using insect wing designs [3–6].

The enhanced flight performance of insects is due to factors such as wake capture, delayed stall, and rotational circulation [7]. Pitch rate damping [8], muscle contraction of the thorax [9], the protein resilin for wing elasticity and flexibility [10–12], and the added wing mass due to the hemolymph [13–15] and vein structure [16, 17] have significant effects on

Handling Editor: Christopher Blanford.

Address correspondence to E-mail: lmtian@jlu.edu.cn; sjy@jlu.edu.cn

https://doi.org/10.1007/s10853-020-05608-0

flight. The structure of the wing vein influences flight performance [18]. The attack angle of the wing flapping of an insect significantly influences its force generation [16, 19, 20], which affects its flight performance. And it must be optimized relative to the wing path in designs for FWMAVs [21].

The flapping wings of tiny insects are the necessary flight organs that undergo twisting and bending deformations [22]. The wing stiffness also depends on the vein pattern and the structure of the veins [23, 24]. The wings of an insect consist of veins, which are made of fibrous materials, and flexible wing membranes [25]. Wing veins are made of six different cuticle layers and epidermal cells [18]. The sandwich structure of the veins can restrict damage diffusion and retain the remaining structure in steady state [26]. The veins of insects can be hollow and filled with hemolymph [15, 27], and the function of unfolding the hindwings is achieved by a hydraulic mechanism [28]. The wing membranes of some insect wings contain a flexion structure and fold lines that often interrupt veins in favor of bending or folding the wing [29], while similar flexion structure also can be found in the pterostigma of some insects.

The analysis of the flight performance of insects uses modeling methods such as conceptual, physical, shell, deformable framework, numerical, and simple analytical models [30]. Attitude kinematics equations are used to analyze the insect flight [31]. The influence of the vein joints of dragonfly wings in flight on passive deformability is dependent on the different structures of the wing [32, 33]. Damage patterns for the sandwich structure of dragonfly veins by struck during experimental observation and numerical predictions indicate that the veins are hollow [26]. The three-dimensional (3-D) models of the libellulid dragonfly (*S. vulgatum*) simulate various microstructural features of sliced sections of veins [34]. The tape-spring-like structure at the surface of the vein is used to fold the hindwings of ladybird beetles [35]. The wings of the fly (*Sarcophaga carnaria*), dragonfly (*Pantala flavescens*), and honeybee (*Apis cerana cerana*) are assumed to be flat plates to analyze their mechanical properties [36]. The static bending tests of the wings of the hawkmoth (*Manduca sexta*) used thin shell elements whose load is set in one direction [37]. The direct study of insects to theoretically calculate flight aerodynamics and construct mechanical models to study insect flight is difficult [38].

In this paper, the relationships between the attack angles, vein structures, and rigidizable behavior of the deployable hindwings of the Asian ladybird (*Harmonia axyridis*) are investigated, which is helpful for designing new MAVs with deployable wing structures. The hemolymph flow in the costa and subcosta anterior (C + ScA) as well as the microstructure of the cross sections of the veins and the wing membranes are observed. Based on veins and the wing membranes structures and dimensions, 3-D models for solid and hollow C + ScA are established. The twisting and bending deformations of the wing models during flight at various attack angles are investigated by ANSYS® software. The relationship between the rigidizable behavior of deployable hindwings and veins is also discussed.

Materials and experimental methods

Biological specimens

Harmonia axyridis were collected from Changchun, China, in March 2020. They were 5–6 mm wide and 6–7 mm long. CO_2 gas was used to euthanize three adult beetle specimens at room temperature; their right hindwings were sliced by sharp razor blades.

Structure of the hindwing and veins

A stereomicroscope (SteREO Discovery V20, Carl Zeiss Microimaging Inc., Germany) was used to determine the outline size and make morphological observations of the whole hindwing in the progression of this study, and these imaging systems provide powerful solutions for observing the structures of the right hindwing. Thus, 3-D models of the hindwing were established. As methods established in Song et al. [15], the hollow structures and dimensions of the veins were got.

The resilin on the C + ScA and around the pterostigma (pst) was obtained by inverted fluorescence microscopy (OLYMPUS DP80, Olympus Optical Co., Ltd., Tokyo, Japan).

Finite element modeling and material properties

The geometric parameters of three hindwings were tested. The average value of vein diameter and wing

membrane thickness was chosen to build the 3-D wing models. This choice is representative because the sizes of the beetles varied. The outline of the wing membrane and the size measurements of the veins were both used to establish the 3-D models of the right hindwing. Considering the structure of the veins, Model I with solid C + ScA venations and Model II with hollow C + ScA venations of the right hindwing were established with Solid Edge. For the comparison of the hindwing vein structures and the attack angles during flight, the flight performances of the models were investigated by ANSYS® software.

The parameters of Model I and Model II were set as follows: the Young's moduli of the wing membrane and veins were 0.9 GPa and 5.17 GPa, respectively [39], and their Poisson's ratios were both set to 0.25 [39]. The elastic modulus of the *H. axyridis* veins ranges from 2.00 to 10.06 GPa [39]. Then, the meshes of Model I and Model II were generated by the ANSYS® software.

Simulation analysis

The statistical analysis of the workbench was used to investigate the flight performance of the right hindwing. The right hindwing models had set loads under the ventral side of C + ScA and all the veins at various attack angles (− 60°, − 30°, 0°, 30° and 60°). The aerodynamic force was set approximately equal to the weight of *H. axyridis* during its hovering flight, 23 mg [39]. The area of the hindwing was approximately 17.48 mm^2. Therefore, the load pressure was set to 6.58 × 10^{-6} MPa, and the supports for Model I with the solid C + ScA and Model II with the hollow C + ScA were fixed at the hindwing root. Then, the deformation tendency of the models at different attack angles was observed, and their flight performances were investigated.

Results

The hemolymph flow and resilin

Figure 1 shows the C + ScA veins with the fluorescent indicator. The brighter sections show the hemolymph flow; the veins of insects are hollow and filled with hemolymph [15, 27]. Hemolymph flows into the hindwing due to accessory pulsatile organs pulling hemolymph from the wing into the thoracic cavity [40]. However, the other *H. axyridis* veins were not hollow. Thus, the C + ScA was assumed to be hollow veins, and the other veins were assumed to be solid veins. The resilin around positions b, c and d is blue in Fig. 1b–d; however, the C + ScA is a brighter blue than the surrounding structure, showing that it has much more resilin. The resilin around the pst is shown in Fig. 1e–g.

Finite element modeling

The outline shape and the various colors of the sections of the hindwing, which were the basic data for the 3-D models of the hindwing, were observed (Fig. 2a). To establish the two models, Model I (hindwing with solid C + ScA) and Model II (hindwing with hollow C + ScA), the data of the diameters of the veins and the thicknesses of the wing membrane were obtained by the wing vein morphology through histological sections, as illustrated in Fig. 2b. To simplify the 3-D models, the shapes of all the veins are assumed to be circular tubes. Based on the slicing experiment of the hindwing, its outline shape and the diameters of the veins were determined. The C + ScA was assumed to be a hollow circular tube, and the other veins were assumed to be solid. The average diameter of all the veins was assumed to be 40 μm, and the wall thickness of the C + ScA was assumed to be 10 μm. The average thickness of the wing membrane was assumed to be 5 μm. The cross sections of the two models showed that the C + ScA was solid veins and hollow veins in Fig. 2c, d, respectively. As shown in Fig. 2f, the pressure loads set on the different models were always set straight up. α represents the attack angle; when pulling up, the angle of the leading edge is positive, and that of the ventral head is negative.

The element sizes of the two models of the wing membrane and veins were both set as 0.008 mm to determine the twisting and bending deformation behavior of the right hindwing and to ensure the necessary element capturing. All the veins were meshed by the hex–dominant method, and the wing membranes were meshed by the automatic method. The total number of elements in Model I and Model II were 2,044,442 and 2,054,945, respectively. Model I and Model II were meshed with 4225230 nodes and 4228958 nodes, respectively.

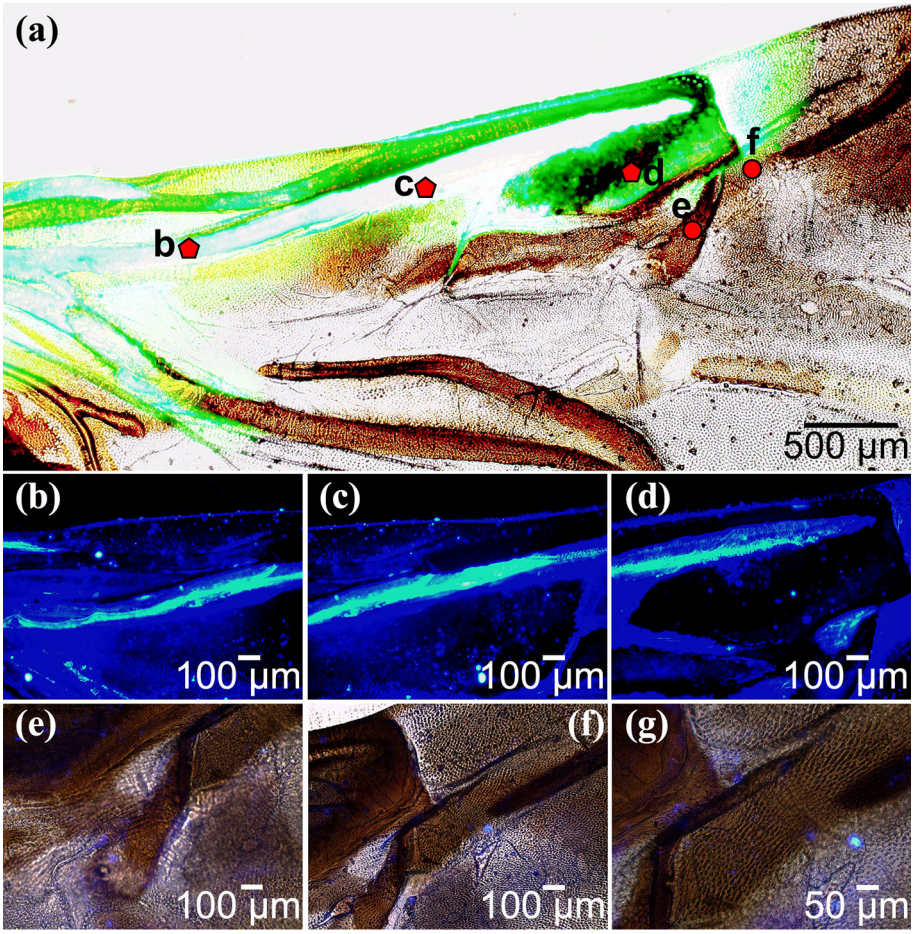

Figure 1 **a** The hemolymph flows through the C + ScA. **b** The resilin observed at position b marked with a red pentagon. **c** The resilin observed at position c marked with a red pentagon. **d** The resilin observed at position d marked with a red pentagon. **e** The resilin observed at position e marked with a red circle. **f** The resilin observed at position f marked with a red circle. **g** The enlarged view of Fig. 1f.

The deformation at different attack angles

When the elytra are lifted high enough during flight, the hindwings will unfold and flap [12]. Figure 3a–e shows the simulation analysis results of the Model I deformations with the loads set under the ventral surface of the C + ScA, and the simulation analysis results of Model II are shown in Fig. 3f–j during flight at various attack angles. The attack angle is optimized relative to the wing path in designs for FWMAVs [21]. As Fig. 3 shows, the maximum deformations of the models occurred at the wing membrane tip, whereas the minimal deformations occurred at the location of the support near the hindwing upper left corner because the pressure is set on the C + ScA. The twisting and bending deformation tendencies of these models were along the load direction.

The deformation trends of these models were similar, whereas the maximum deformations were different. Figure 4a–e shows the total deformations of the simulation analysis result of Model I, whose loads were exerted under the ventral surface of all the veins during flight at different attack angles (− 60°, − 30°, 0°, 30° and 60°). The stroke angle of the hindwing ranges approximately from 160° to 170° [41]. Thus, the lateral angle of attack of the flapping wing of *H. axyridis* is − 60° to 60°. The simulation analysis results of Model II are shown in Fig. 4f–j. The maximum deformations of the models are at the ventral right corner of the wing membrane. Due to the pressures set on all the veins, the hindwing experienced changing deformations. Figures 3 and 4 show that the bending and twisting deformation tendencies of the models are focused along the direction of the pressure loading. Due to the attack angle and the vein structure of hind wing various, the deformation trend of the right hindwing models and maximum deformations are changed. These results show that veins have the most important effect on the flight performance of *H. axyridis* and can shift the hindwing deformation trend in flight.

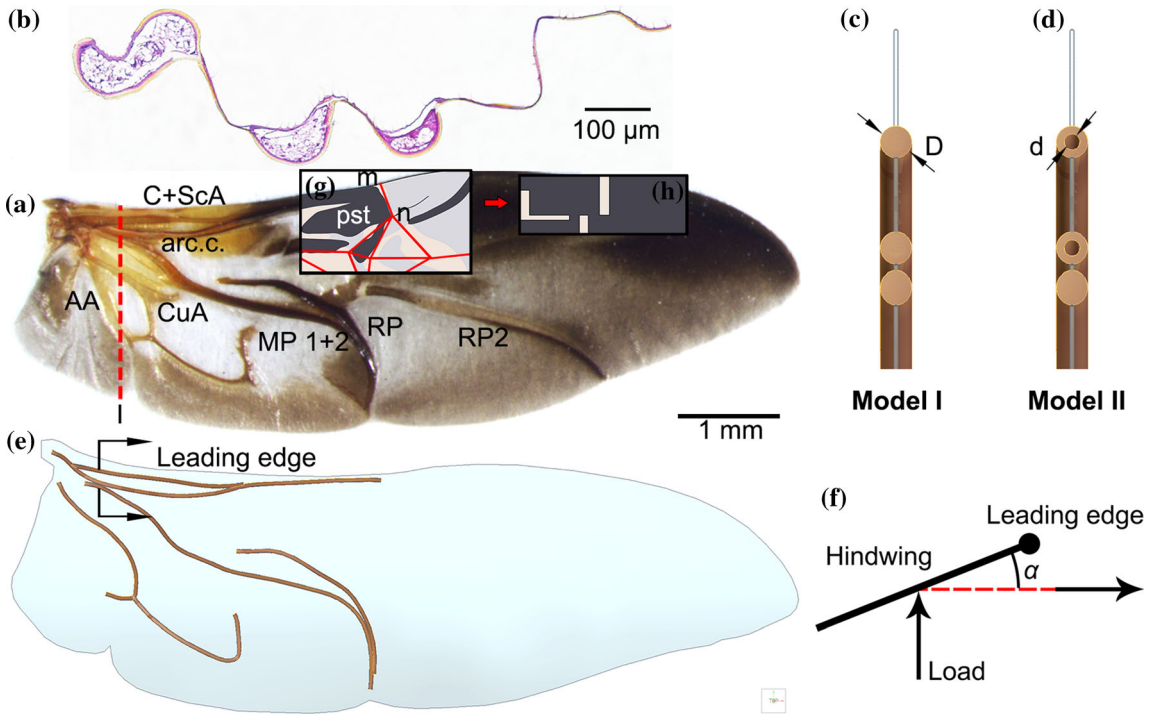

Figure 2 **a** *H. axyridis* hindwing. **b** The cross section with hematoxylin–eosin staining cut at location I along the red line. **c** Model I (hindwing with solid C + ScA). **d** Model II (hindwing with hollow C + ScA). **e** Hindwing model. **f** The flight force diagram with the load set straight up; α is the attack angle. **g** The black frame: a partial view of the hindwing. The dark gray represents the main veins, and the pale gray represents the false vein. The other areas represent the wing membrane. The red lines are folding lines. **h** Simplified model of **g**. The HE staining process included dewaxing, hematoxylin staining, hydrochloric acid alcohol differentiation, weak ammonia water returning orchid, eosin staining, dehydration, and neutral gum sealing [15].

As Figs. 3 and 4 show, the simulation analysis results of the models whose loads were set under the ventral surface of the veins at the attack angle of 0° showed the maximum deformations, which were 210.8 μm and 49.4 μm for the hollow and solid C + ScA, respectively. As all of the main veins were under a load, with the C + ScA only under pressure, the maximum deformation due to the load under the ventral surface of all of the veins was 4.27 times that of only the C + ScA. Thus, the hindwing where each of the veins is under pressure experienced a larger load force.

Figure 5 shows the variation in the deformation of the models whose loads were exerted on different veins as sinusoidal functions with different attack angles (− 60°, − 30°, 0°, 30° and 60°), demonstrating that the variation trends of the maximum deformation y of the four models were almost consistent with the attack angle x and the sinusoidal fitting of x and y, as follows:

$$y_1 = -0.59 + 47.21 \sin\left(\pi \frac{x + 91.54}{183.04}\right) \quad (1)$$

$$y_2 = 3.60 + 45.79 \sin\left(\pi \frac{x + 87.15}{174.30}\right) \quad (2)$$

$$y_3 = 9.09 + 191.36 \sin\left(\pi \frac{x + 88.24}{176.48}\right) \quad (3)$$

$$y_4 = 37.42 + 173.38 \sin\left(\pi \frac{x + 81.08}{162.15}\right) \quad (4)$$

where x is the attack angle and y is the maximum deformation in units of μm. The coefficient of determination R^2 illustrates the goodness of fit of a curve, and the R^2 values of the sinusoidal fitting curves of y are as follows: $R_1^2 = 0.998$, $R_2^2 = 0.999$, $R_3^2 = 0.999$ and $R_4^2 = 0.998$.

As Fig. 5 shows, the four models had the same trend of maximum deformation with the angle of attack and location of pressure. Larger deformations of the hindwing always occurred in the model with a hollow C + ScA. The hollow veins had a much

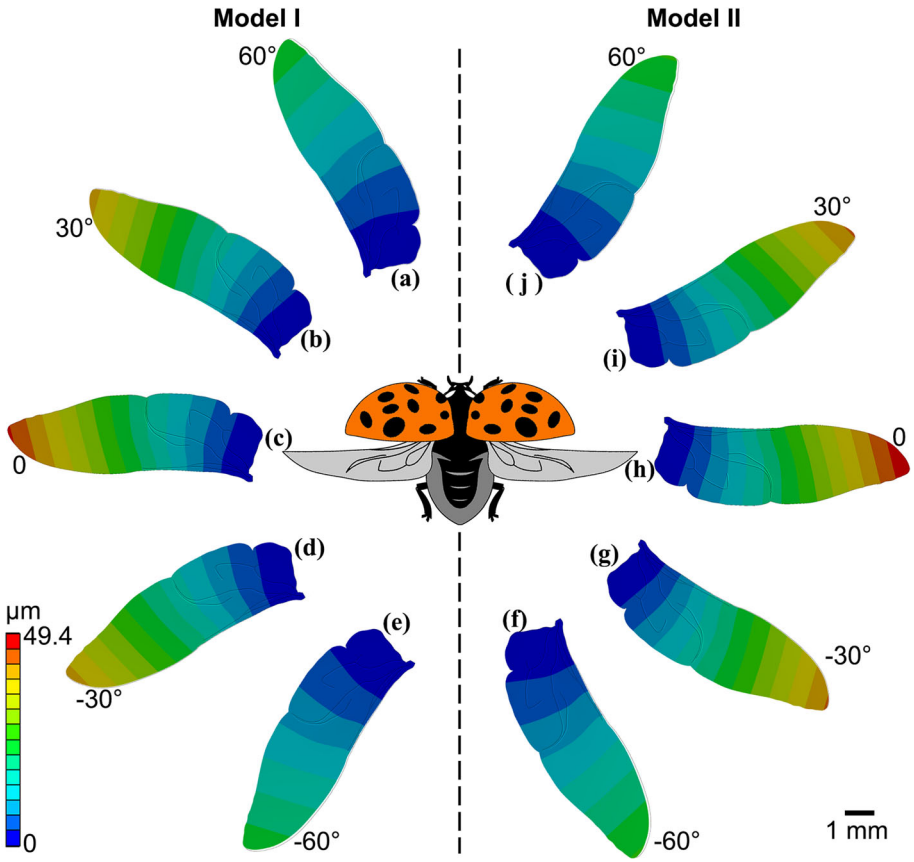

Figure 3 Simulation analysis results of Model I and Model II, whose loads were set under the ventral surface of the C + ScA at different attack angles (− 60°, − 30°, 0°, 30° and 60°) during flight.

higher flexibility, and the solid veins had a much higher stability.

The bar graphs in Figs. 6 and 7 show the relations of the maximum equivalent elastic strain and the maximum equivalent stress of the simulation analysis results of the right hindwings, respectively, with attack angles of − 60°, − 30°, 0°, 30° and 60°.

The two bar graphs show that the relations of the maximum equivalent elastic strain and the maximum equivalent stress in the simulation analyses result from the deformation tendency of the − 60°, − 30°, 0°, 30° and 60° attack angles. The equivalent stress of the solid C + ScA is less than the hollow vein set pressure on the C + ScA. A change in the vein structures of the hindwing will change the stress conditions. Each vein is a function of flight deformation, and the coupled motions of all the veins on the twisting and bending deformations during flight are very important.

Discussion

The hindwing and veins

The added wing mass due to the hemolymph [13, 14] and vein structure [16] has significant effects on flight. The vein structure may be hollow or solid, and the hemolymph flows through the hollow veins. Hemolymph is necessary for numerous sensory structures and live tissues in the wing, and through hydraulic pressure, it is responsible for opening and closing the foldable beetle hindwings [42, 43]. The addition of hindwing mass also changes the natural frequency of the hindwing [39]. Thus, the hemolymph helps control the flight performance of the hindwing [15].

The wings of an insect consist of veins, which are made of fibrous materials, and flexible wing membranes [25]. Some main veins support the wing membrane; these veins are mostly in the first half section [44]. The veins with dark color (which can be observed in the wing) may only be bent, without folding and unfolding, to ensure the stability of the hindwing because not all veins have the folding

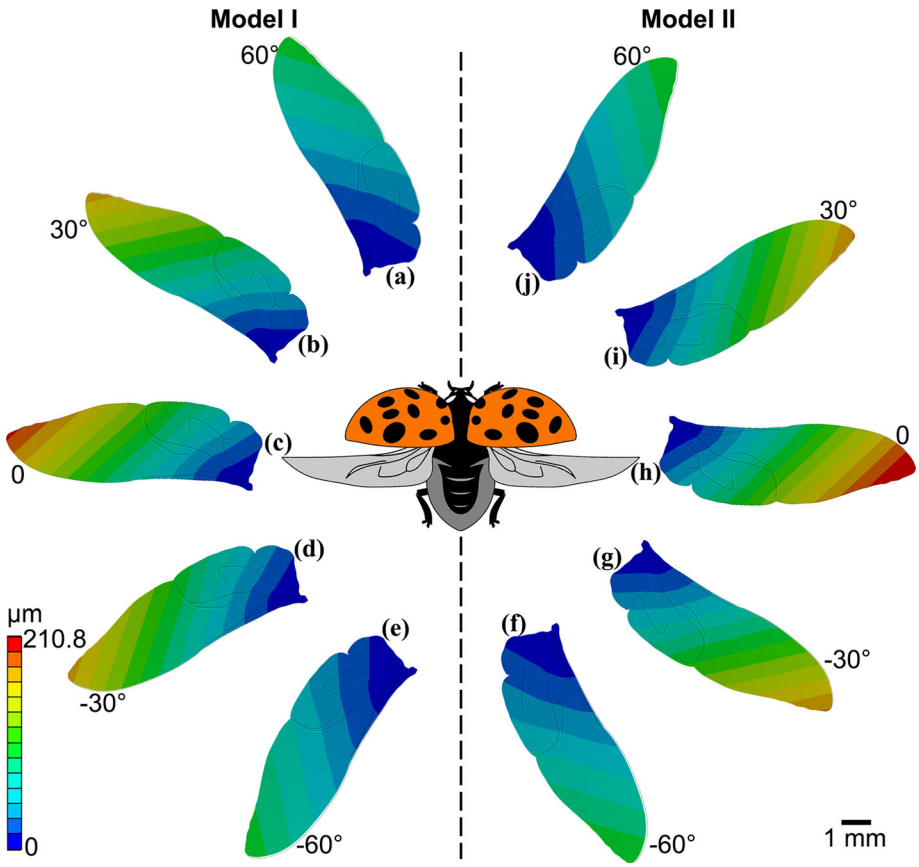

Figure 4 Simulation analysis results of Model I and Model II, whose loads are set under the ventral surface of all the veins at different attack angles (− 60°, − 30°, 0°, 30° and 60°) during flight.

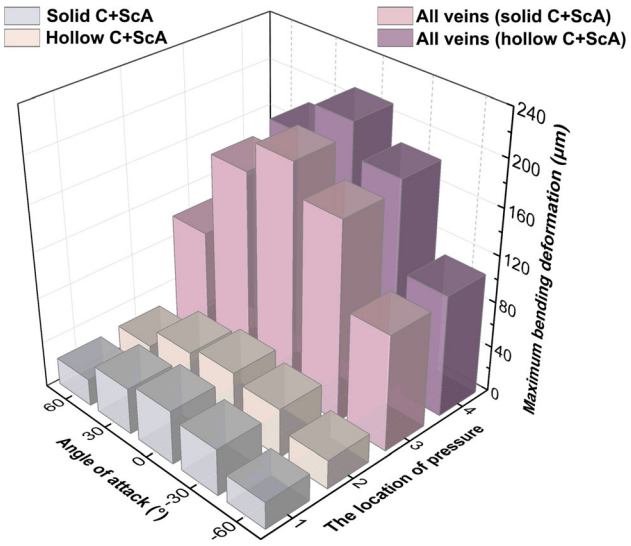

Figure 5 The maximum deformations of the simulation analysis results of Model I and Model II, whose loads are set under the ventral face of the C + ScA, with all veins, at different attack angles (− 60°, − 30°, 0°, 30° and 60°) during flight.

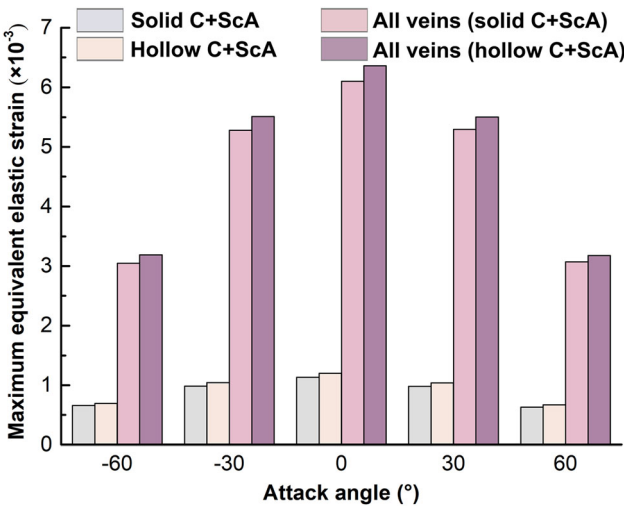

Figure 6 The maximum equivalent elastic strains of the simulation analysis results of Model I and Model II, whose loads are set under the ventral face of the C + ScA, with all veins, at different attack angles (− 60°, − 30°, 0°, 30° and 60°) during flight.

function. The wing membrane is a composite material with a high tensile strength [11]. In contrast, the light color sections and the dark color sections both play roles in the flight performance of the twisting and bending deformation behaviors and the folding/unfolding mechanisms of the right hindwing.

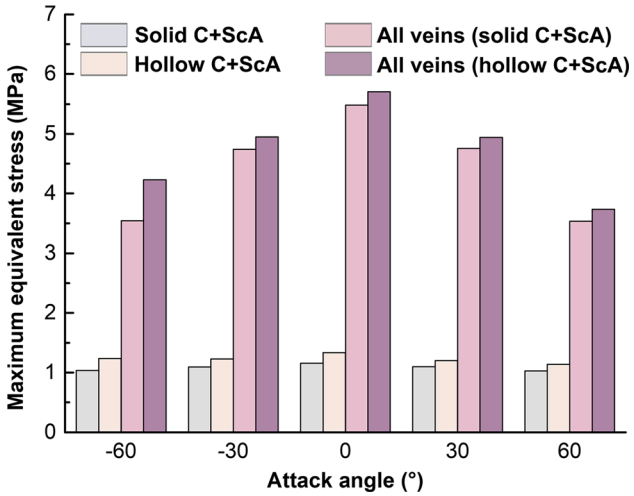

Figure 7 The maximum equivalent stresses of the simulation analysis results of Model I and Model II, whose loads are set under the ventral face of the C + ScA, with all veins, at different attack angles (− 60°, − 30°, 0°, 30° and 60°) during flight.

The structures of the veins influence the flight performance [18]. The major veins include the nerve and trachea [40], which can control the hindwings. The false veins of the hindwing are almost curved and exhibit the folding and unfolding function [35]. Their structure and shape in the cross sections may be helpful for determining their twisting and bending deformations during flight and their folding/unfolding mechanism. The wing stiffness also depends on the vein pattern and the structure of the veins [23, 24]. The cross sections of the wing membrane, which can be used to study both the unfolding/folding mechanism and the flight performance for the hindwing, form irregular half-circles. The wrinkle structure on the hindwing is helpful for folding [17]. The resilin acts as the energy storage material for folding and unfolding the hindwing [11]. The reduced modulus of different veins is also helpful for folding the hindwing [17]. The vein structure is critical for the design of the deployable wings of MAVs.

The rigidizable behavior of deployable hindwings

Resilin, a superelastic protein, is embedded in arthropod exoskeletons, especially in insect wings which is helpful for the wing elasticity and flexibility, and capable of elastic energy storage [10–12]. Due to the fluoresces, Fig. 1b–d show that the C + ScA has much brighter blue color than the other regions which means it has much more resilin. The structures that allow wing folding, built-in creases in the membrane and vein joints, can be damaged; however, the embedded resilin found throughout wing veins can resist that damage [11]. The C + ScA is bent when the hindwing is folded, and it is helpful for the hindwing to unfold [11]. The C + ScA is the main vein for hindwing flapping. The pst is located at the end of the C + ScA. The pst has no resilin, but the resilin surrounds it, as shown in Fig. 1d–g, because pst adds mass to the hindwing to decrease the natural frequency of the hindwing, which is helpful for flight [39], while the structures around the pst are helpful for folding/unfolding of the hindwing.

The line mn in Fig. 2a is the folding line, and it is located on the margin of the hindwing. The area around point m exhibits different folding structures, such as the bending zone, folding patch, and marginal joint [45]. However, these folding structures are not observed at m because this position may only fold, without bending deformation, during folding of the hindwing. This position is not folded during flight, and torsion also occurs during flapping flight. The vein distributions are the main factor for maintaining hindwing unfolding. The main veins are also linked with each other or the false veins so that the hindwing can maintain a stable condition during flapping flight.

Based on the simplified model of Fig. 2h, six comparative models are established. The tested thicknesses of the vein (T_v) are 20 μm and 10 μm, and the tested thicknesses of the membrane (T_m) are 20 μm and 10 μm, respectively. The element sizes of the six models are set as 0.01 mm to more clearly observe the deformation behavior. All the models are meshed with the hex dominant method. The total amounts of the elements of the six models are 20519, 19369, 20819, 10468, 201819 and 10468. These models are meshed with 116522, 111421, 114904, 72992, 114904 and 72992 nodes, respectively. The force set on the models is 2.3×10^{-5} N to induce bending deformation, and the torque is 1.05×10^{-4} N·mm to induce twisting deformation. The simulation results are shown in Figs. 8 and 9.

The simulation results show that the rigidizable material can change the deformation tendency, unlike the uniform materials of other parts. The membrane exhibits a flexible deformation that is greater than the flexible deformation of other parts,

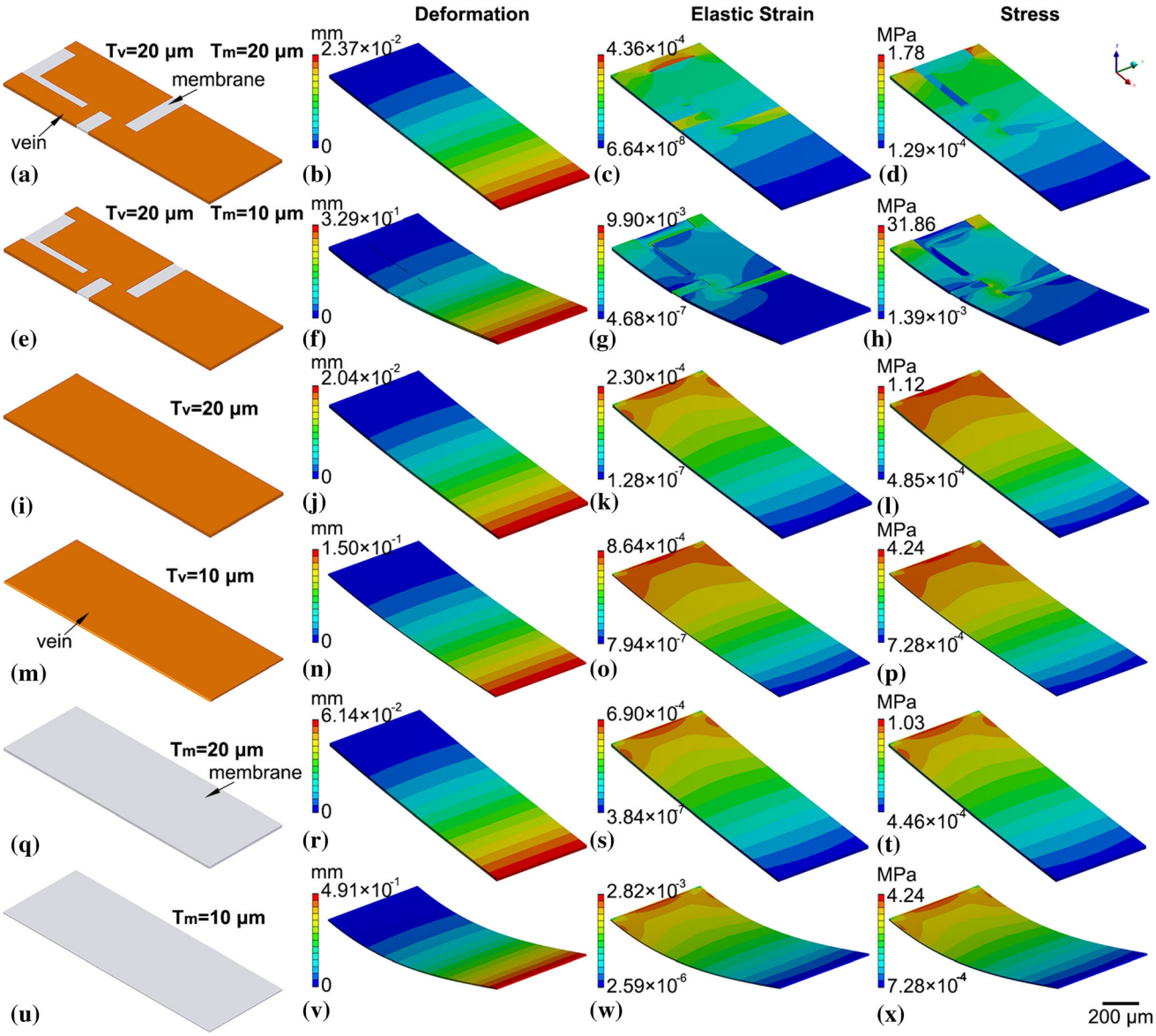

Figure 8 Bending deformation of the six models. **a** Complex I (vein and membrane with the same greater thickness). **b** Deformation, **c** elastic strain, **d** stress of Complex I. **e** Complex II (vein and membrane with different thicknesses). **f** Deformation, **g** elastic strain, and **h** stress of Complex II. **i** Vein I (thicker). **j** Deformation, **k** elastic strain, **l** stress of Vein I. **m** Vein II (thinner). **n** Deformation, **o** elastic strain, and **p** stress of Vein II. **q** Membrane I (thicker). **r** Deformation, **s** elastic strain, and **t** stress of membrane I. **u** Membrane II (thinner). **v** Deformation, **w** elastic strain, and **x** stress of membrane II.

but this structure may be damaged easily. The vein structure has higher stability than the other models, but it does not contribute to folding the hindwing. Thus, the complex membrane and vein structures interact to allow stable flight and folding/unfolding of the hindwing. The vein structure supporting the membrane keeps the hindwing stable, and the membrane increases in area, which is helpful for stable flight and folding/unfolding the hindwing many times with resilin. The rigidizable behavior of deployable hindwings is a significant factor for both flight performance and the necessary folding/unfolding mechanism.

The deformation at different attack angles

The flapping angle is taken to be 60°, which is a representative average value for Odonata flapping amplitudes. The angle of attack of the wing during flapping is assumed to be 30° on average for both the

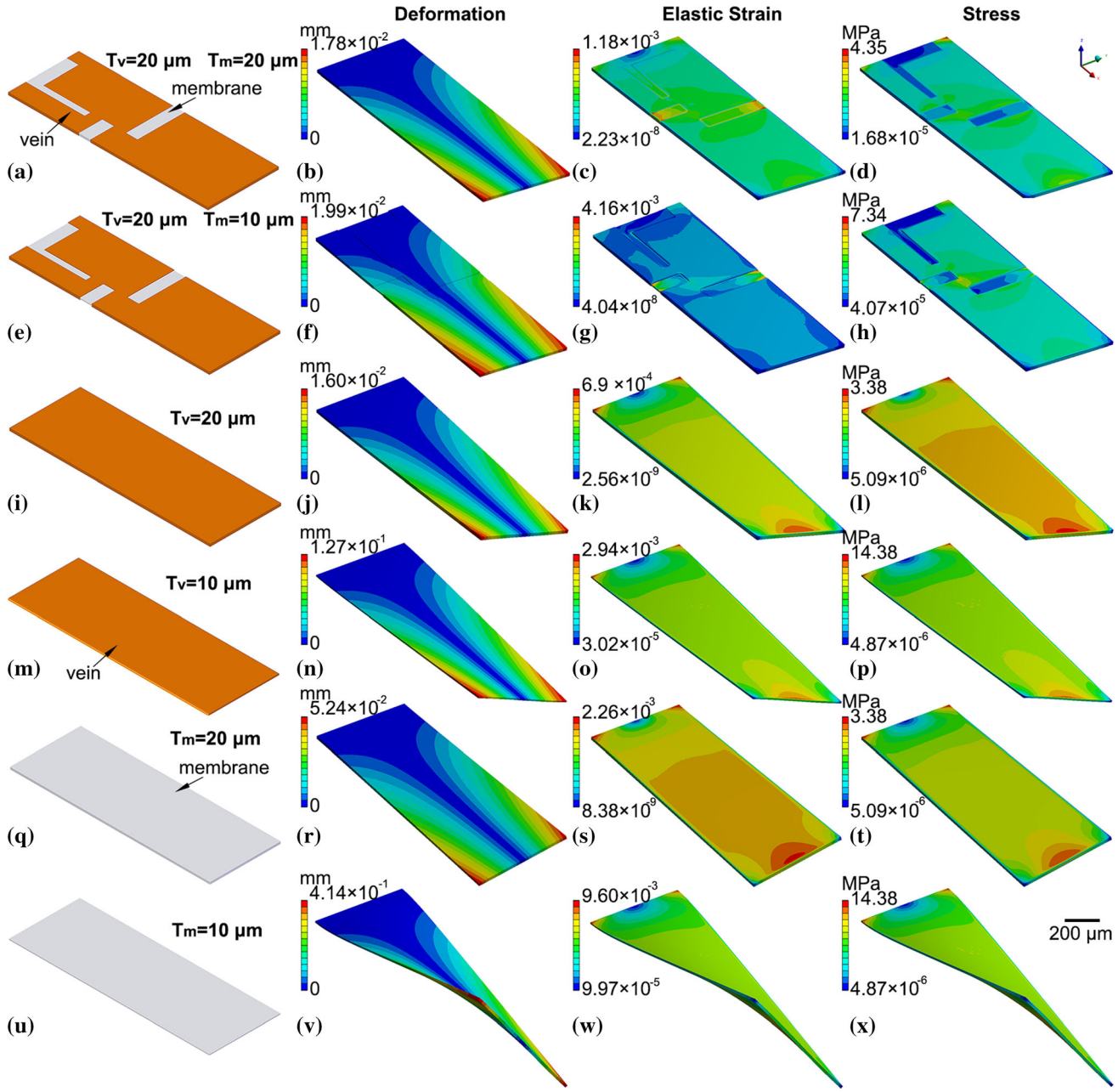

Figure 9 Twisting deformation of the six models. **a** Complex I (vein and membrane with the same greater thickness). **b** Deformation, **c** elastic strain, **d** stress of Complex I. **e** Complex II (vein and membrane with different thicknesses). **f** Deformation, **g** elastic strain, **h** stress of Complex II. **i** Vein I (thicker). **j** Deformation, **k** elastic strain, **l** stress of Vein I. **m** Vein II (thinner). **n** Deformation, **o** elastic strain, and **p** stress of Vein II. **q** Membrane I (thicker). **r** Deformation, **s** elastic strain, and **t** stress of membrane I. **u** Membrane II (thinner). **v** Deformation, **w** elastic strain, and **x** stress of membrane II.

up- and downstroke, which is estimated based on values found for several insects [46]. The magnitudes of the deformations of the models at attack angles of ± 30° are almost equivalent, as are the values at attack angles of ± 60°. The maximum deformations of the models occur at an attack angle of 0°, as shown in Fig. 3. The minimum deformations of the right hindwings are observed at attack angles ± 60°. Thus, the deformation has a relationship with the attack angle. The change in the attack angle during wing flapping influences the production of force [16, 19].

The magnitudes of the deformation of the right hindwings at attack angles of ± 30° and ± 60° are almost equivalent. As Fig. 4 shows, the maximum

deformations of the models are observed at the attack angle of 0°. However, the minimum deformations are observed at attack angles ± 60°. Because the hindwing is supported by all of the veins [12], their twisting and bending deformations extend from the ventral right margin to the end of the hindwing root. The maximum deformations are observed at the posterior margins, and the deformation trends are the same for the two models. However, the maximum deformations of the two models begin at different locations of the wingtip, and the minimum deformations always occur at the hindwing root. Because the wing root positions have muscles for flight, they are always moving. The deformations of all the veins under pressure are homogenous, so each vein of the hindwing plays a significant role in the hindwing twisting and bending deformations.

The deformations of the models with a set pressure on all the veins are more uniform than those with a set pressure on only the C + ScA. The analysis results show that the C + ScA plays an important role in flight performance. The hindwing may possess the function of self-adaption, which is helpful for flight performance, and the different deformations of the hindwing are caused by the different attack angles.

The airflow that contacts the surface of the hindwing generates lift force, which is used to support the insect's flapping flight [16]. The magnitudes of the twisting and bending deformations of the models of the two situations are different because the same pressures affect the ventral surfaces of different veins. The veins play significant roles in the twisting and bending deformations of the hindwings, so they can influence the flight performance of the hindwings. Thus, the deformation tendencies are along the component direction of force. When different areas of the veins are affected, the load force on the veins varies.

With increasing mass, the natural frequency of the hindwing decreases [15]. The mass of the hindwing with hollow veins is lighter than that with solid veins, so the solid veins can decrease the natural frequency of the hindwing. The reduced modulus of a vein has little influence on the natural frequency of the hindwing [17]. Thus, the mass may be the major influencing factor on the natural frequency of the hindwing. Each vein is an influencing factor of flight performance, and the coupled motions of all the veins on the twisting and bending deformations during flight play a positive role in its flapping motion.

The deflection of a vein is w_B:

$$w_B = \frac{Fl^3}{3EI} \tag{5}$$

where F is the load force, l is the distance between the location of the load set and root, E is Young's modulus, and I is the moment of inertia.

The moment of inertia of a solid vein is I_{P1}:

$$I_{P1} = \int_0^{D/2} \rho^2 \cdot 2\pi\rho \mathrm{d}\rho \tag{6}$$

$$I_{P1} = \frac{\pi}{32} D^4 \tag{7}$$

where D is the outer diameter of the vein.

The deflection of a solid vein is w_{B1}:

$$w_{B1} = \frac{32Fl^3}{3E\pi D^4} \tag{8}$$

The moment of inertia of a hollow vein is I_{P2}:

$$I_{P2} = \int_{d/2}^{D/2} \rho^2 \cdot 2\pi\rho \mathrm{d}\rho \tag{9}$$

$$I_{P2} = \frac{\pi}{32}\left(D^4 - d^4\right) \tag{10}$$

where d is the inner diameter of the hollow vein.

The deflection of a hollow vein is w_{B2}:

$$w_{B2} = \frac{32Fl^3}{3E\pi\left(D^4 - d^4\right)} \tag{11}$$

Thus, the deflection ratio between a solid vein and a hollow vein is as follows:

$$\frac{w_{B1}}{w_{B2}} = \frac{D^4 - d^4}{D^4} \tag{12}$$

$$\frac{w_{B1}}{w_{B2}} = 1 - \frac{d^4}{D^4} < 1 \tag{13}$$

The hollow vein undergoes a greater deformation than the solid vein. The magnitudes of the deformations of the veins are the same for the same magnitude of force at different attack angles. However, the deformation of the hindwing changes with the attack angle, which may be caused by the structure of the hindwing. The loads are applied to the veins, and they are linked with the wing membrane. Thus, the veins will impact the deformation of the hindwing.

The wing membrane is also a stiffener, which can change the mechanical properties. The complex structures of the wing membrane and veins are the important parts supporting hindwing flight.

The attack angle is optimized relative to the wing path in designs for FWMAVs [21]. The deformation of the hindwing during flight has a sinusoidal relationship with the attack angle. The attack angle plays a significant role in deformation; thus, it is a significant factor for analyzing the effect of veins on flight performance and the total hindwing deformation during flight. To design the attack angle of an MAV flapping wing, the total weight is also considered, as it is critical for the design of the body of the MAV.

The attack angle and the vein structure both play important roles in flight performance. Biological systems can be used for devising biomimetic structures based on their excellent physical, mechanical, sensing, and optical capabilities [47, 48]. A comparison of the simulation analysis results proves that each vein plays a significant role in the twisting and bending deformation; analysis of their mechanical properties is essential for devising the wing flapping attack angles for MAVs.

Conclusions

The Asian ladybird beetle (*Harmonia axyridis*) shows that very small Coleoptera are capable of flight through deployable hindwings, which feature flight stability and folding/unfolding mechanisms. Considering the rigidizable behavior without refolding during flight, the relationship between the rigidizable behavior of deployable hindwings and vein structure is investigated. The wing membranes are assumed to be the same thickness, and the veins are also assumed to be circular tubes of the same diameter for the design of 3-D models so that workbench software could be used to study the structural properties of the veins and the wing membrane and the resulting hindwing deformation properties. The flight performance of the hindwing deformation is studied considering the comparison between the hollow C + ScA of the hindwing as a natural structure and solid C + ScA. The hollow veins are flexible, and the sinusoidal fitting curve of the deformations and attack angles motivates biomimetic design and function and inspires the bionic engineering of the flapping performance of the wings of biomimetic MAVs.

Acknowledgements

This work was supported by the National Natural Science Foundation of China (Grant Number 31970454), the Young and Middle-aged Technology Innovation Leading Talents and Team Projects of Science and Technology Development Plan of Jilin Province (Grant No. 20200301013RQ), the China-EU H2020 FabSurfWAR Project (Grant Number 644971), the 111 Project (B16020) of China, the China Scholarship Council (CSC), and Graduate Innovation Fund of Jilin University.

Author contributions

ZLS and JYS designed the study; ZLS and YWY coordinated the study; ZLS, JT, LMT, and JYS conducted the research and analyzed the data; ZLS wrote the manuscript; and LMT and JYS reviewed the manuscript, discussed the results, and gave final approval for publication.

Compliance with ethical standards

Conflict of interest The authors declare that there are no conflicts of interest to disclose.

Ethical standards This work complies with the ethical guidelines of Jilin University.

References

[1] Takizawa K, Tezduyar TE, Buscher A (2015) Space–time computational analysis of MAV flapping-wing aerodynamics with wing clapping. Comput Mech 55:1131–1141. https://doi.org/10.1007/s00466-014-1095-0

[2] Phan HV, Au TKL, Park HC (2016) Clap-and-fling mechanism in a hovering insect-like two-winged flapping-wing micro air vehicle. R Soc Open Sci 3:160746. https://doi.org/10.1098/rsos.160746

[3] Phan HV, Kang T, Park HC (2017) Design and stable flight of a 21 g insect-like tailless flapping wing micro air vehicle with angular rates feedback control. Bioinspir Biomim 12:1–17. https://doi.org/10.1088/1748-3190/aa65db

[4] Nguyen Q-V, Chan WL, Debiasi M (2015) Performance tests of a hovering flapping wing micro air vehicle with double wing clap-and-fling mechanism. J Bionic Eng 13:235–248

[5] Truong QT, Argyoganendro BW, Park HC (2014) Design and demonstration of insect mimicking foldable artificial wing using four-bar linkage systems. J Bionic Eng 11:449–458. https://doi.org/10.1016/S1672-6529(14)60057-3

[6] Jitsukawa T, Adachi H, Abe T, Yamakawa H, Umezu S (2017) Bio-inspired wing-folding mechanism of micro air vehicle (MAV). Artif Life Robot 22:203–208. https://doi.org/10.1007/s10015-016-0339-9

[7] Dickinson MH (1999) Wing rotation and the aerodynamic basis of insect flight. Science (80-) 284:1954–1960. https://doi.org/10.1126/science.284.5422.1954

[8] Taylor GK (2003) Dynamic flight stability in the desert locust Schistocerca gregaria. J Exp Biol 206:2803–2829. https://doi.org/10.1242/jeb.00501

[9] Hou D, Zhong Z, Yin Y, Pan Y, Zhao H (2017) The role of soft vein joints in dragonfly flight. J Bionic Eng 14:738–745. https://doi.org/10.1016/S1672-6529(16)60439-0

[10] Rajabi H, Ghoroubi N, Stamm K, Appel E, Gorb SN (2017) Dragonfly wing nodus: a one-way hinge contributing to the asymmetric wing deformation. Acta Biomater 60:330–338. https://doi.org/10.1016/j.actbio.2017.07.034

[11] Song Z, Yan Y, Tong J, Sun J (2020) Asian ladybird folding and unfolding of hind wing: biomechanical properties of resilin in affecting the tensile strength of the folding area. J Mater Sci 55:4524–4537. https://doi.org/10.1007/s10853-019-04326-6

[12] Haas F, Gorb S, Blickhan R (2000) The function of resilin in beetle wings. Proc R Soc Lond Ser B Biol Sci 267:1375–1381. https://doi.org/10.1098/rspb.2000.1153

[13] Hou D, Yin Y, Zhao H, Zhong Z (2015) Effects of blood in veins of dragonfly wing on the vibration characteristics. Comput Biol Med 58:14–19. https://doi.org/10.1016/j.compbiomed.2014.12.018

[14] Hou D, Yin Y, Zhong Z, Zhao H (2015) A new torsion control mechanism induced by blood circulation in dragonfly wings. Bioinspir Biomim 10:016020. https://doi.org/10.1088/1748-3190/10/1/016020

[15] Song Z, Tong J, Yan Y, Wu W, Sun J (2020) Effects of microfluid in the veins of the deployable hindwings of the Asian ladybeetle on flight performance. Comput Biol Med 121:103817. https://doi.org/10.1016/j.compbiomed.2020.103817

[16] Wang X, Zhang Z, Ren H, Chen Y, Wu B (2017) Role of soft matter in the sandwich vein of dragonfly wing in its configuration and aerodynamic behaviors. J Bionic Eng 14:557–566. https://doi.org/10.1016/S1672-6529(16)60421-3

[17] Song Z, Tong J, Yan Y, Wu W, Tian L, Sun J (2021) Combined effects of wrinkled vein structures and nanomechanical properties on hind wing deformation. Micron 140:102965. https://doi.org/10.1016/j.micron.2020.102965

[18] Appel E, Heepe L, Lin CP, Gorb SN (2015) Ultrastructure of dragonfly wing veins: composite structure of fibrous material supplemented by resilin. J Anat 227:561–582. https://doi.org/10.1111/joa.12362

[19] Van TT, Nguyen QV, Lee H (2017) Bio-inspired flexible flapping wings with elastic deformation. Aerospace 4:1–26. https://doi.org/10.3390/aerospace4030037

[20] Dong H, Bode-Oke AT, Li C (2018) Learning from nature: unsteady flow physics in bioinspired flapping flight. In: Flight physics—models, techniques and technologies. InTech

[21] Ellington CP (1999) The novel aerodynamics of insect flight: applications to micro-air vehicles. J Exp Biol 202:3439–3448

[22] Mountcastle AM, Daniel TL (2009) Aerodynamic and functional consequences of wing compliance. Exp Fluids 46:873–882. https://doi.org/10.1007/s00348-008-0607-0

[23] Wootton RJ (1993) Leading edge section and asymmetric twisting in the wings of flying butterflies. J Exp Biol 180:105–117

[24] Combes SA (2003a) Flexural stiffness in insect wings I. Scaling and the influence of wing venation. J Exp Biol 206:2979–2987. https://doi.org/10.1242/jeb.00523

[25] Bao XQ, Bontemps A, Grondel S, Cattan E (2011) Design and fabrication of insect-inspired composite wings for MAV application using MEMS technology. J Micromech Microeng 21:125020. https://doi.org/10.1088/0960-1317/21/12/125020

[26] Arjangpay A, Darvizeh A, Yarmohammad Tooski M, Ansari R (2018) An experimental and numerical investigation on low velocity impact response of a composite structure inspired by dragonfly wing configuration. Compos Struct 184:327–336. https://doi.org/10.1016/j.compstruct.2017.10.006

[27] Zhao H, Yin Y, Zhong Z (2013) Arnold circulation and multi-optimal dynamic controlling mechanisms in dragonfly wings. Acta Mech Solida Sin 26:237–244. https://doi.org/10.1016/S0894-9166(13)60022-1

[28] Sun J, Ling M, Wu W, Bhushan B, Tong J (2014) The hydraulic mechanism of the unfolding of hind wings in *Dorcus titanus platymelus* (Order: Coleoptera). Int J Mol Sci 15:6009–6018. https://doi.org/10.3390/ijms15046009

[29] Hedrick TL, Combes SA, Miller LA (2015) Recent developments in the study of insect flight. Can J Zool 93:925–943. https://doi.org/10.1139/cjz-2013-0196

[30] Wootton RJ, Herbert RC, Young PG, Evans KE (2003) Approaches to the structural modelling of insect wings. Philos Trans R Soc London Ser B Biol Sci 358:1577–1587. https://doi.org/10.1098/rstb.2003.1351

[31] Zuo D, Chen W, Peng S, Zhang W (2006) Modeling and simulation study of an insect-like flapping-wing micro aerial vehicle. Adv Robot 20:807–824. https://doi.org/10.1163/156855306777681393

[32] Rajabi H, Ghoroubi N, Darvizeh A, Appel E, Gorb SN (2016) Effects of multiple vein microjoints on the mechanical behaviour of dragonfly wings: numerical modelling. R Soc Open Sci 3:150610. https://doi.org/10.1098/rsos.150610

[33] Rajabi H, Ghoroubi N, Darvizeh A, Dirks J, Appel E, Gorb SN (2015) A comparative study of the effects of vein-joints on the mechanical behaviour of insect wings: I. Single joints. Bioinspir Biomim 10:056003. https://doi.org/10.1088/1748-3190/10/5/056003

[34] Rajabi H, Shafiei A, Darvizeh A, Dirks JH, Appel E, Gorb SN (2016) Effect of microstructure on the mechanical and damping behaviour of dragonfly wing veins. R Soc Open Sci 3:160006. https://doi.org/10.1098/rsos.160006

[35] Saito K, Nomura S, Yamamoto S, Niyama R, Okabe Y (2017) Investigation of hindwing folding in ladybird beetles by artificial elytron transplantation and microcomputed tomography. Proc Natl Acad Sci 114:5624–5628. https://doi.org/10.1073/pnas.1620612114

[36] Tong J, Chang Z, Yang X, Zhang J, Liu X, Chetwynd DG, Chen D, Sun J (2015) Nanoindentation mechanical properties and structural biomimetic models of three species of insects wings. J Wuhan Univ Technol Sci Ed 30:831–839. https://doi.org/10.1007/s11595-015-1238-y

[37] Combes SA (2003b) Flexural stiffness in insect wings II. Spatial distribution and dynamic wing bending. J Exp Biol 206:2989–2997. https://doi.org/10.1242/jeb.00524

[38] Sane SP (2003) The aerodynamics of insect flight. J Exp Biol 206:4191–4208. https://doi.org/10.1371/journal.pone.0186441

[39] Song Z, Tong J, Yan Y, Sun J (2020) Effects of pterostigma structure on vibrational characteristics during flight of Asian ladybird *Harmonia axyridis* (Coleoptera: Coccinellidae). Sci Rep 10:11371. https://doi.org/10.1038/s41598-020-68384-6

[40] Arnold JW (1964) Blood circulation in insect wings. Mem Entomol Soc Canada 96:5–60. https://doi.org/10.4039/entm9638fv

[41] Le TQ, Van TT, Park SH, Quang TT, Ko JH, Park HC, Byun D (2013) Improvement of the aerodynamic performance by wing flexibility and elytra–hind wing interaction of a beetle during forward flight. J R Soc Interface 10:20130312. https://doi.org/10.1098/rsif.2013.0312

[42] Pass G (2018) Beyond aerodynamics: the critical roles of the circulatory and tracheal systems in maintaining insect wing functionality. Arthropod Struct Dev 47:391–407. https://doi.org/10.1016/j.asd.2018.05.004

[43] Hillyer JF, Pass G (2020) The insect circulatory system: Structure, function, and evolution. Annu Rev Entomol 65:121–143. https://doi.org/10.1146/annurev-ento-011019-025003

[44] Sun J, Song Z, Pan C, Liu Z (2018) Analysis of light-mass and high-strength veins of hind wing from Asian ladybird beetle. In: 2018 IEEE international conference on manipulation, manufacturing and measurement on the nanoscale (3M-NANO). IEEE, pp 142–145

[45] Haas F (2006) Evidence from folding and functional lines of wings on inter-ordinal relationships in Pterygota. Arthropod Syst Phylogeny 64:149–158

[46] Jongerius SR, Lentink D (2010) Structural analysis of a dragonfly wing. Exp Mech 50:1323–1334. https://doi.org/10.1007/s11340-010-9411-x

[47] Aizenberg J, Fratzl P (2013) New materials through bioinspiration and nanoscience. Adv Funct Mater 23:4398–4399. https://doi.org/10.1002/adfm.201302690

[48] Chen P-Y, McKittrick J, Meyers MA (2012) Biological materials: functional adaptations and bioinspired designs. Prog Mater Sci 57:1492–1704. https://doi.org/10.1016/j.pmatsci.2012.03.001